

We are IntechOpen, the world's leading publisher of Open Access books Built by scientists, for scientists

6,900

Open access books available

186,000

International authors and editors

200M

Downloads

Our authors are among the

154

Countries delivered to

TOP 1%

most cited scientists

12.2%

Contributors from top 500 universities



WEB OF SCIENCE™

Selection of our books indexed in the Book Citation Index
in Web of Science™ Core Collection (BKCI)

Interested in publishing with us?
Contact book.department@intechopen.com

Numbers displayed above are based on latest data collected.
For more information visit www.intechopen.com



Magnetization Dynamics–Induced Charge and Spin Transport on the Surface of a Topological Insulator Subjected to Magnetism

Katsuhisa Taguchi

Additional information is available at the end of the chapter

<http://dx.doi.org/10.5772/62531>

Abstract

We theoretically show spin and charge transport on the disordered surface of a three-dimensional topological insulator with a magnetic insulator when localized spin of the magnetic insulator depends on time and space. To ascertain the transports, we use a low-energy effective Hamiltonian on the surface of a topological insulator using the exchange interaction and calculate analytically using Green's function techniques within the linear response to the exchange interaction. As a result, the time-dependent localized spin induces the charge and spin current. These currents are detected from change in the half-width value of the ferromagnetic resonance of the localized spin when the magnetic resonance of the localized spin is realized in the attached magnetic insulator. We also show spin and charge current generation in a three-dimensional Weyl–Dirac semimetal, which has massless Dirac fermions with helicity degrees of freedoms. The time-dependent localized spin drives the charge and spin current in the system. The charge current as well as the spin current in the Weyl–Dirac system are slightly different from those on the surface of the topological insulator.

Keywords: Spin pumping, Spin–momentum locking, Surface of topological insulator, Weyl–Dirac semimetal, Massless Dirac fermions

1. Introduction

A crucial issue in spintronics is the generation and manipulation of a charge and spin current by magnetism, since these mechanisms can be applicable to magnetic devices. One way to generate charge and spin flow is called “spin pumping,” which pumps from the angular

momentum of a magnetization's localized spin into that of electrons through the dynamics of magnetization as well as spin-orbit interactions [1, 2]. No other way of doing this has so far been discussed in the field of metallic spintronics.

Ever since the discovery of a topological insulator (TI) [3–6], spintronics using topology has been studied. A TI has a gapless surface, its bulk is insulating, but its surface is metallic as a result of two-dimensional massless Dirac fermions on the surface [4–6]. Because of spin–orbit interactions on the surface the spin and momentum of Dirac fermions are perfectly linked to each other. The relation between a TI's spin and momentum is dubbed “spin–momentum locking,” and the direction in which they travel is perpendicular to each other. Because of spin–momentum locking, unconventional spin-related phenomena—such as magnetoresistance [7–15], the magnetoelectric effect [16–21], diffusive charge–spin transport [22–25], and the spin pumping effect [26–31]—have so far been the only phenomena theoretically and experimentally studied.

Of the unconventional phenomena on the surface of a TI, spin pumping is one of the most interesting when it comes to spintronics. Here spin pumping on the surface is different from that in metals. As a result of spin–momentum locking on the surface the localized spin plays the role of a vector potential, whereas time-differential localized spin effectively plays the role of an electric field acting on electrons on the surface of the TI [16–19]. As a result, even in the absence of an applied electric field, the charge current is generated by time-dependent localized spin as shown in **Figure 1**. The induced charge current flows along $\mathbf{z} \times \partial_t \mathbf{S}$ [28–31]. Actually, this spin pumping effect on the surface has been experimentally demonstrated in the junction of the TI by attaching magnetic materials [29–31] by changing the half-width value when ferromagnetic resonance is realized in the attached magnetic material [32, 33].

Recently, it has been reported that localized spin on the surface of a TI subject to magnetism depends on space and its spin texture seems to be a magnetic domain wall [34]. It is predicted that in the presence of a spatial-dependent spin structure the charge current, which reflects the spin structure, is induced [28]. Moreover, the spin current as well as the charge density are induced when an inhomogeneous spin structure exists on the surface. Detailed results are shown in Section 2. This study may help the study of spin pumping on the surface of a TI with inhomogeneous spin textures [35, 36].

Recently, the next generation of spintronics has been theoretically and experimentally studied in Weyl–Dirac semimetals. A Weyl–Dirac semimetal possessing three-dimensional massless Dirac fermions has attracted much attention in condensed matter physics [37–39]. Such a semimetal has been experimentally demonstrated [40–45]. In addition, Weyl–Dirac semimetals have been theoretically predicted in a superlattice heterostructure based on the TI. Such a heterostructure has been realized in the GeTe/Sb₂Te₃ superlattice [46].

Spin-momentum locking occurs in a Weyl–Dirac semimetal, but the locking is slightly different from that on the surface of the TI. As a result of spin–momentum locking, the spin polarization (charge density) and the charge current (spin current) are linked to each other. Moreover, Dirac fermions have helicity degrees of freedom, which are decomposed into left- and right-handed fermions. Note that the total charge flow of Dirac fermions of left- and right-handed Weyl

fermions is preserved. In a Weyl–Dirac semimetal the anomaly-related effect, which is discussed in the field of relativistic high-energy physics, has also been discussed in condensed matter physics. Studies up to the moment have asserted that the charge current is generated by magnetic properties with helicity degrees of freedoms [47–54]. Our goal is to introduce the helicity-dependent spin pumping effect, one of the characteristic properties of Dirac fermions (as shown in Section 3).

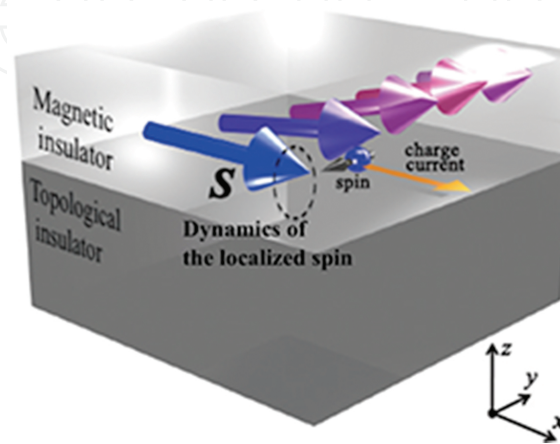


Figure 1. Schematic of spin pumping on the surface of a topological insulator with localized spins of the attached magnetic insulator. Here, the localized spin depends on positions on the surface. The dynamics of the localized spin (dashed line) drives the charge current (orange arrow) on the surface. Then, the charge current is also polarized because of spin–momentum locking on the surface.

2. Spin and charge transport due to spin pumping on the surface of a topological insulator

2.1. Model

We will calculate the charge and spin current due to spin pumping on the surface of a TI with an attached magnetic insulator (MI) (as illustrated in **Figure 1**). To do so, we consider the following low-energy effective Hamiltonian, which describes the surface of the TI with localized spin of the MI [4]:

$$H = H_{\text{TI-surface}} + H_{\text{ex}} + H_{\text{imp}}, \quad (1)$$

where $H_{\text{TI-surface}}$, H_{ex} , and H_{imp} are the low-energy effective Hamiltonian on the surface of the TI, the spin–exchange interaction between the localized spin of the attached MI and the spin of conduction electrons, and the nonmagnetic impurity scattering on the surface of the TI, respectively. $H_{\text{TI-surface}}$ is given by

$$\sum_{\mathbf{k}} \psi_{\mathbf{k}}^{\dagger} [-\hbar v_{F,B} (\bar{\mathbf{k}} \times \bar{\boldsymbol{\sigma}})_z - E_F] \psi_{\mathbf{k}}. \quad (2)$$

where $v_{F,B}$, E_F , \mathbf{k} , and $\boldsymbol{\sigma}$ are the velocity of bare electrons, the Fermi energy, momentum on the surface of the TI, and the Pauli matrix in the spin space, respectively; and $\Psi_{\mathbf{k}} = {}^t(\Psi_{\uparrow}, \Psi_{\downarrow})$ and Ψ^{\dagger} are the annihilation and creation operators of the electrons with up-spin and down-spin index (\uparrow, \downarrow). H_{ex} is represented by

$$H_{\text{ex}} = -J_{\text{ex}} \int dx^2 \psi^{\dagger} (\bar{\mathbf{S}} \cdot \bar{\boldsymbol{\sigma}}) \psi. \quad (3)$$

where J_{ex} is the coefficient of the exchange interaction; and \mathbf{S} is the localized spin of the MI on the surface. Here, we take into account the space- and time-dependence of \mathbf{S} . H_{imp} is given by

$$H_{\text{imp}} = \int dx^2 \psi^{\dagger} u_{\text{imp}} \psi \quad (4)$$

Nonmagnetic impurity scattering is taken into account for a delta function type [19, 21–24] and is considered within the Born approximation. Because of impurity scattering the Fermi velocity of bare Dirac fermions in Eq. (2) is modified by $v_{F,B} \rightarrow v_F$ [23, 24, 28]. We use v_F in what follows.

2.2. Charge and spin current due to localized spin dynamics

We will calculate the charge and spin current as well as the charge and spin density due to magnetization dynamics on the surface of the TI. They are given using the Keldysh–Green function and the lesser component of Green's function [48] as

$$\begin{aligned} \langle j^i(x, t) \rangle &= ev_F \langle \psi^{\dagger}(x, t) \sigma^i \psi(x, t) \rangle = -i \frac{\hbar}{2\pi} ev_F \text{tr}[\sigma^i G^<(x, t; x, t)] = \frac{ev_F}{2} \langle s^i \rangle, \\ \langle j_{s,\alpha}^i(x, t) \rangle &= \frac{1}{2} v_F \varepsilon^{z\alpha i} \langle \psi^{\dagger}(x, t) \psi(x, t) \rangle = -\frac{i\hbar}{h} v_F \varepsilon^{z\alpha i} \text{tr}[G^<(x, t; x, t)] = \frac{v_F}{2e} \varepsilon^{z\alpha i} \langle \rho \rangle. \end{aligned} \quad (5)$$

As a result of spin–momentum locking the charge current $\langle j^i \rangle$ and spin current $\langle j_{s,\alpha}^i \rangle$ are proportional to the spin density $\langle s^i \rangle$ and charge density $\langle \rho \rangle$, respectively, where $\langle \rangle =$ denotes the expectation value in H and $e(\langle 0 \rangle)$ is the charge of Dirac fermions. These relations are derived from the Heisenberg equation. The superscript and subscripts in $\langle j_{s,\alpha}^i \rangle$ show the direction of flow and spin of the spin current, respectively. In what follows the charge and spin current are considered within the linear response to H_{ex} . This assumption can be a good approximation because the energy scale of the exchange interaction is smaller than that of the bandwidth of the low-energy effective Hamiltonian on the surface of the TI [28, 31]. We also assume the TI has a metallic surface of and that a finite Fermi surface exists on the surface; that is, $\hbar/(E_F \tau) \ll 1$ where \hbar is the Planck constant and τ is the relaxation time of nonmagnetic impurity scatterings on the surface.

The charge and spin current are represented by

$$j^i(x, t) = \frac{ie\hbar v_F J_{\text{ex}}}{L^2} \sum_{\vec{q}, \Omega} e^{i(\Omega t - \vec{q} \cdot \vec{x})} \text{tr}[\sigma^i \Pi^j(\vec{q}, \Omega)] S_{\vec{q}, \Omega}^j, \quad (6)$$

$$j_{s,\alpha}^i(x, t) = \frac{i\hbar v_F J_{\text{ex}}}{2L^2} \varepsilon^{z\alpha i} \sum_{\vec{q}, \Omega} e^{i(\Omega t - \vec{q} \cdot \vec{x})} \text{tr}[\Pi^j(\vec{q}, \Omega)] S_{\vec{q}, \Omega}^j,$$

where \vec{q} and Ω are the momentum and frequency of the localized spin $S_{\vec{q}, \Omega}^j$, respectively; L^2 is the area of the surface; and Π^j is the response function. These currents are obtained from Π^j :

$$\Pi^j(\vec{q}, \Omega) = \sum_{\omega, \vec{k}} (f_{\omega+\Omega/2} - f_{\omega-\Omega/2}) g_{\omega-\Omega/2, \vec{k}-\vec{q}/2}^R \Lambda^j(\vec{q}, \Omega) g_{\omega+\Omega/2, \vec{k}+\vec{q}/2}^A \quad (7)$$

where $f_{\omega} g_{\omega, \vec{k}}^R = ([g_{\omega, \vec{k}}^A]^\dagger) = [h\omega/(2\pi) + E_F - \hbar v_F/(2\pi)(\vec{k} \times \sigma)_z + i\hbar/(4\pi\tau)]^{-1}$, and Λ^j are the Fermi distribution function, the retarded (advanced) Green function, and the vertex correction of the ladder diagram, respectively. The above functions are estimated in the regime $\Omega\tau \ll 1$ and $qv_F\tau \ll 1$, which are satisfied when the dynamics of the localized spin is lower than the terahertz regime and the spatial gradient of the localized spin is slow compared with the electron mean free path. Then, by expanding Ω and q within $\Omega\tau \ll 1$ and $qv_F\tau \ll 1$, the vertex function Λ^j is represented by $\Lambda^j = [\Gamma + \Gamma^2 + \Gamma^3 + \dots]^{jn} \sigma^n = [(1 - \Gamma)^{-1}]^{jn} \sigma^n$ with

$$\Gamma^j \equiv n_c u_i^2 \sum_{\omega, \vec{k}} g_{\omega-\Omega/2, \vec{k}-\vec{q}/2}^R \sigma^j g_{\omega+\Omega/2, \vec{k}+\vec{q}/2}^A = \Gamma^{jn} \sigma^n. \quad (8)$$

where Γ^{jn} ($|\Gamma^{jn}| < 1$) is the 3×3 matrix ($j, n = 0, x, y$). As a result, Π^j is given by

$$\begin{pmatrix} \Pi^0 \\ \Pi^x \\ \Pi^y \end{pmatrix} = -\frac{\Omega}{2\pi} \begin{pmatrix} l & i|q_y| & -i|q_x| \\ \frac{l}{q^2|l^2 + i\Omega\tau} & \frac{i|q_y|}{q^2|l^2 + i\Omega\tau} & \frac{-i|q_x|}{q^2|l^2 + i\Omega\tau} \\ \frac{ilq_y}{q^2|l^2 + i\Omega\tau} & l - \frac{q^2|l^2}{2(q^2|l^2 + i\Omega\tau)} & \frac{q_x q_y |l^2}{q^2|l^2 + i\Omega\tau} \\ \frac{-i|q_x|}{q^2|l^2 + i\Omega\tau} & \frac{q_x q_y |l^2}{q^2|l^2 + i\Omega\tau} & l - \frac{q^2|l^2}{2(q^2|l^2 + i\Omega\tau)} \end{pmatrix} \begin{pmatrix} \sigma^0 \\ \sigma^x \\ \sigma^y \end{pmatrix} \quad (9)$$

where σ^0 is the identity matrix; and l is the mean free path on the surface. From Eqs. (5–9) the spin and charge current are given by

$$\begin{aligned}\langle j^i \rangle &= -2ev_e^{\text{TI}} J_{\text{ex}} v_F \tau \left((\vec{z} \times \partial_t \bar{S}^{\parallel})^i - \ell^2 [\vec{z} \times (\vec{z} \times \vec{\nabla})] [\vec{\nabla} \times \partial_t \langle \bar{S}^{\parallel} \rangle_{\text{D}}]_z \right), \\ \langle j_{s,\alpha}^i \rangle &= \varepsilon^{z\alpha i} v_e^{\text{TI}} J_{\text{ex}} v_F \ell^2 [\vec{\nabla} \times \partial_t \langle \bar{S}^{\parallel} \rangle_{\text{D}}]_z,\end{aligned}\quad (10)$$

where v_e^{TI} is the density of state on the surface of the TI; $\langle S^{\parallel} \rangle_{\text{D}}$ is the convolution between S^{\parallel} and the diffusion propagator D on the surface; and S^{\parallel} is the in-plane localized spin $S^{\parallel} = S - S^z \mathbf{z}$ as

$$\begin{aligned}\langle \bar{S}^{\parallel} \rangle_{\text{D}} &\equiv \frac{1}{\tau} \int_{-\infty}^{\infty} dt' \int dx' D(x - x', t - t') \bar{S}^{\parallel}(x', t'), \\ D(x - x', t - t') &= \frac{1}{L^2} \sum_{\vec{q}, \Omega} \frac{1}{q^2 v_F \tau + i\Omega} e^{i(\Omega t - \vec{q} \cdot \vec{x})}.\end{aligned}\quad (11)$$

Eq. (10) shows that time-dependent localized spin induces the charge and spin current and that they can be decomposed into local and nonlocal contributions. The first term in Eq. (10) is the charge current due to spin dynamics at that position on the surface; its direction is along the $\mathbf{z} \times \partial_t S^{\parallel}$ direction [28–31]. On the other hand, the second term in Eq. (10) is the charge current due to both time- and spatial-dependent localized spin; its direction is along the $[\mathbf{z} \times (\mathbf{z} \times \partial)] [\partial \times \partial_t \langle S^{\parallel} \rangle_{\text{D}}]_z$ direction, where $\langle S^{\parallel} \rangle_{\text{D}}$ indicates the nonlocal contribution from the localized spin. Moreover, this term is zero when the spin texture is spatially uniform. Therefore, this charge current is caused by diffusion with the dynamics of the spatial inhomogeneous spin texture. It is noted that this second term is also described by the spatial gradient of the charge density.

Because of spin–momentum locking on the surface of the TI, spin polarization is given by $\langle \mathbf{j} \rangle = 2ev_F(\mathbf{z} \times \langle \mathbf{s} \rangle)$. Thus, the properties of spin polarization are similar to those of the charge current.

Eq. (11) shows that the spin current is induced by the time- and spatial-dependent S^{\parallel} . Then, the charge density is also generated because of spin–momentum locking. In addition, the second term of the charge current $\langle \mathbf{j} \rangle_{\text{nonlocal}} = 2ev_F v_e^{\text{TI}} J_{\text{ex}} \tau \ell^2 [\mathbf{z} \times (\mathbf{z} \times \partial)] [\partial \times \partial_t \langle S^{\parallel} \rangle_{\text{D}}]_z$ is given by the spatial gradient of the charge density, whereas $\langle \mathbf{j} \rangle_{\text{nonlocal}}$ is proportional to the spatial gradient of the spin current [28] as

$$\langle j^i \rangle_{\text{nonlocal}} = -e\ell \varepsilon^{z\alpha n} \nabla^i \langle j_{s,\alpha}^n \rangle. \quad (12)$$

This result shows that the relation between the charge and spin current is different from that in the metallic spintronics system [2]. The spin current is proportional to the charge current and spin current flow is perpendicular to the charge flow and its spin polarization.

Note that no out-of-plane localized spin $S^z \mathbf{z}$ contributes in a dominant way to charge and spin current generation. The reason is σ^z does not couple with momentum \mathbf{p} in Eq. (2). Therefore,

we believe a warping effect [1–4] on the surface of the TI is likely. Spin polarization along the z -direction is also generated by spin dynamics.

2.3. Spin torque

Based on these results, we look at localized spin dynamics after generation of the charge current and spin polarization on the surface [24]. We assume there is an external static and AC magnetic field on the surface—as shown in **Figure 2(a)**. The static magnetic field arranges the localized spin texture and the AC magnetic field triggers its spin dynamics. The propagation direction of the microwave is parallel to the static magnetic field, which is along the y -axis. The texture is called the “longitudinal conical spin order” [56].

After applying the microwave the dynamics of the localized spin of the MI is induced by the in-plane AC magnetic field of the microwave. The dynamics of the spin induces the charge and spin current. Then, from $\langle j \rangle = 2ev_F(z \times \langle s \rangle)$, Eq. (10), and spin–momentum locking, spin polarization is also generated. Note that spin polarization induced in this way acts on the localized spin as an effective exchange field for localized spin. This contribution is given from the Landau–Lifshitz–Gilbert (LLG) equation of motion [32, 33] on the surface of the TI:

$$\partial_t \vec{M} \equiv -\gamma\mu(\vec{M} \times \vec{H}) + \frac{\alpha_G}{M}(\vec{M} \times \partial_t \vec{M}) + \vec{T}_e \quad (13)$$

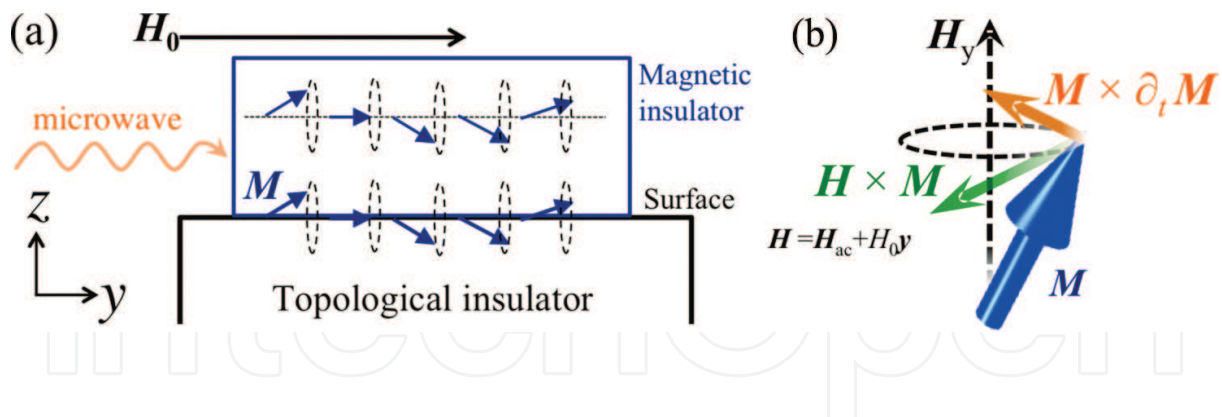


Figure 2. (a) Schematic of the setup used to detect spin and charge current generation. The texture of the magnetization M depends on space. Such magnetization is along the applied static magnetic field H_0 , and the magnetization dynamics is induced by the applied magnetic field of the microwave. (b) Schematic of the spin torque acting on M .

where $M = -M(S/S)$ is magnetization of the MI; γ is the gyromagnetic ratio; μ is permeability; α_G is a Gilbert damping constant; $H = H_0 + H_{AC}$ are the applied magnetic fields on the surface; and H_0 and H_{ac} denote the static and AC magnetic fields, respectively. The first term of Eq. (13) denotes the field-like torque that drives the dynamics of M . The second term is the damping torque that prevents its dynamics—these terms are schematically illustrated in **Figure 2(b)**.

The third term T_e is the spin torque due to spin polarization of Dirac fermions on the surface of the TI ($\langle s \rangle$). It is given by $T_e = 2J_{\text{ex}} a^2 (\mathbf{M} \times \langle s \rangle)$, where a is the lattice constant on the surface.

Since T_e is proportional to $\langle s \rangle$, this torque is decomposed into local (T_e^L) and nonlocal spin torque (T_e^D) terms as

$$\begin{aligned}\bar{T}_e^L &= \frac{\kappa}{M^{\parallel}} \bar{\mathbf{M}} \times \partial_t \bar{\mathbf{M}}^{\parallel}, \\ \bar{T}_e^D &= \frac{\kappa}{M^{\parallel}} \ell^2 \bar{\mathbf{M}} \times (z \times \bar{\nabla}) (\bar{\nabla} \times \partial_t \langle \bar{\mathbf{M}}^{\parallel} \rangle_D)_z,\end{aligned}\quad (14)$$

where $M^{\parallel} = -M(S^{\parallel}/S)$ is in-plane magnetization; and κ is the dimensionless coefficient.

As a result of spin-momentum locking the torque is $T_e \sim \mathbf{M} \times \langle \mathbf{j} \rangle$. This relation is useful as a way of detecting nonzero $\langle \mathbf{j} \rangle$ [29–31]. Moreover, nonlocal spin torque can be described by $T_e^D \sim \mathbf{M} \times \langle \mathbf{j} \rangle_{\text{nonlocal}}$. Eq. (12) shows this torque may well be affected by spin current contribution, whereas the relation between spin torque and spin current can be used as a way to detecting $\langle j_{s,\alpha}^i \rangle$ on the surface:

$$\bar{T}_e^D = \frac{J_{\text{ex}} \tau a^2}{\hbar} \varepsilon^{zai} \bar{\mathbf{M}} \times [(z \times \bar{\nabla}) (\bar{\nabla} \times \langle j_{s,i}^a \rangle)]. \quad (15)$$

We now consider magnetization when it is given by $\mathbf{M} = (M_x, M_y, M_z) = [m \cos(\mathbf{q} \cdot \mathbf{x} - \Omega t), M_y, m \sin(\mathbf{q} \cdot \mathbf{x} - \Omega t)]$ with $\mathbf{q} = (q_x, q_y)$, $m^2 \ll M_y$, $M_y \sim M$, and $\partial_t M_y \sim 0$. Such a time-dependent magnetic structure is assumed to be realized when the magnitude of the static magnetic field is larger than that of the AC magnetic field $H_{\text{AC}} = (h_x, 0, h_z)$; that is, $h_x, h_z \ll H_0$. Then, substituting this \mathbf{M} into Eqs. (13) and (14), the LLG equation becomes a linear approximation:

$$\begin{aligned}\partial_t m_x &= \omega_H m_z - \omega_M h_z + \alpha_G \partial_t m_z, \\ \partial_t m_z &= -\omega_H m_x + \omega_M h_x - (\alpha_G + \kappa) \partial_t m_z + \kappa q_y^2 \partial_t \langle M^{\parallel,x} \rangle_D,\end{aligned}\quad (16)$$

where $\omega_H = \gamma \mu H$ and $\omega_M = \gamma \mu M$ are the angular frequencies of H_0 and M , respectively; and $\kappa q_y^2 \partial_t \langle M^{\parallel,x} \rangle_D$ indicates the contribution from T_e^D . Substituting $\langle M^{\parallel,x} \rangle_D$ into Eq. (13), we obtain magnetic permeability around the surface:

$$\begin{pmatrix} m_x \\ m_z \end{pmatrix} = \begin{pmatrix} \chi_{xx} & \chi_{xz} \\ \chi_{zx} & \chi_{zz} \end{pmatrix} \begin{pmatrix} h_x \\ h_y \end{pmatrix} \quad (17)$$

where χ_{xx} and χ_{zx} denote the longitudinal and transverse magnetic permeability as

$$\begin{aligned}\chi_{xx}(q, \Omega) &= \frac{(\omega_H + i\alpha\Omega)\omega_M}{[\omega_H + i\alpha\Omega][\omega_H + i(\alpha\tilde{k}_{q,\Omega})\Omega] - \zeta_{q,\Omega}\Omega^2}, \\ \chi_{zz}(q, \Omega) &= \frac{\omega_H + i(\alpha + \tilde{k}_{q,\Omega})\Omega}{\omega_H + i\alpha\Omega} \chi_{xx}(q, \Omega), \\ \chi_{xz}(q, \Omega) &= -\zeta_{q,\Omega}\chi_{xx}(q, \Omega) = -\chi_{zx}.\end{aligned}\tag{18}$$

The coefficients $\kappa'_{q,\Omega}$ and $\zeta_{q,\Omega}$ are given by

$$\kappa'_{q,\Omega} = \kappa \left(1 - \frac{q^4 l^4}{q^4 l^4 + \Omega^2 \tau^2} \right), \quad \zeta_{q,\Omega} = 1 + \kappa \frac{q^2 l^2 \Omega \tau}{q^4 l^4 + \Omega^2 \tau^2}.\tag{19}$$

Hence, $\kappa'_{q,\Omega}$ and $\zeta_{q,\Omega}$ depend on q and Ω . If $q = 0$, $\kappa'_{q,\Omega}$ and $\zeta_{q,\Omega}$ go to $\kappa'_{q,\Omega} \rightarrow \kappa$ and $\zeta_{q,\Omega} \rightarrow 1$, respectively. Then, the magnetic permeability is isotropic. In $q = 0$, χ_{xx} and χ_{zz} go to the same value and $\chi_{xz} = -\chi_{zx}$ is satisfied. On the other hand, in nonzero q the magnetic permeability is anisotropic: $\chi_{xx} \neq \chi_{zz}$.

Figure 3(a) shows the dependence of Ω on the imaginary part of the longitudinal magnetic permeability for several q . The resonance frequency Ω_r and the half-width value $\Delta\Omega$ are slightly changed by the nonzero q . **Figure 3(b)** shows change in the resonance frequency for several f_H in greater detail— f_H is the frequency described by the static magnetic field H_0 . The resonance frequency decreases with increasing ql from $ql = 0$ into $ql = q_0 l$, where q_0 satisfies $q_0^2 l^2 \sim \Omega\tau$. In

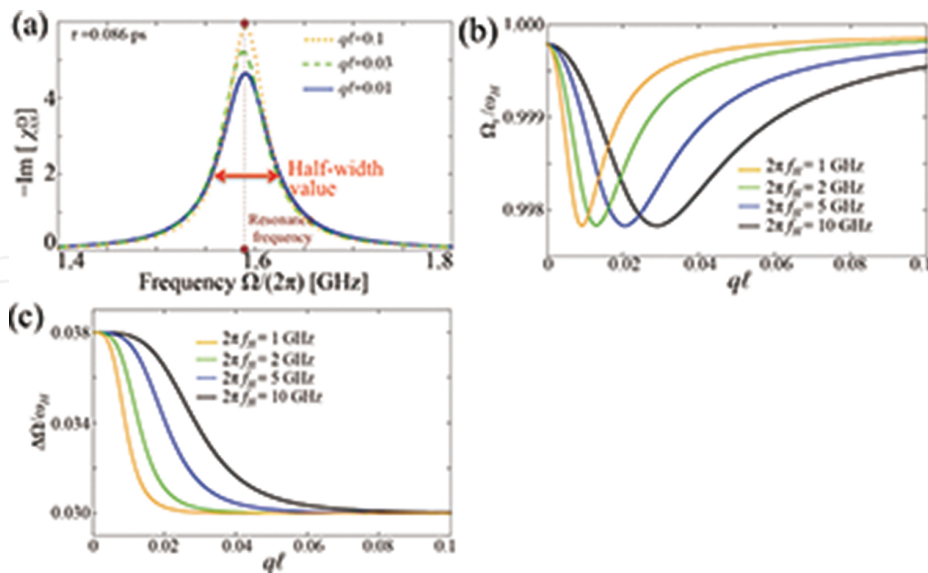


Figure 3. (a) Frequency dependence of the imaginary part on the longitudinal magnetic permeability of several ql . The half-width value and resonance frequency change according to ql . (b) Dependence of ql on the resonance frequency for several frequencies of the applied static magnetic field. (c) Dependence of ql on the half-width of several frequencies of the static magnetic field [49].

addition, when ql takes a large value the resonance frequency returns to that frequency at $ql=0$. **Figure 3(c)** shows the momentum dependence of the half-width value on renormalization by the angular frequency of the applied magnetic field for several $\omega_H = 2\pi f_H$ frequencies when realistic parameters on the surface of the TI are taken into account [31]. Change in the normalized half-width value $\Delta\Omega/\omega_H(ql)$ decreases from $\Delta\Omega/\omega_H(ql=0) = 0.038$ to $\Delta\Omega/\omega_H(ql \sim 0.1) = 0.030$ with increasing ql .

Any change in the half-width value $\Delta\Omega$ indicates an induced charge current on the surface of the TI because $T_e^L + T_e^D$ is proportional to the induced charge current [29–31]. In addition, the half-width value $\Delta\Omega$ of T_e^D represents a contribution from the spatial gradient of the spin current. These relations can be useful for the detection of spin current. For example, let us suppose that in a finite ql , $\Delta\Omega$ includes the contribution from the whole of the spin torque T_e and the contribution from the nonlocal term T_e^D is reduced by the large magnetic field. In a higher magnetic field the inhomogeneous spin texture would be expected to be aligned along the magnetic field direction and the spin texture to be spatially uniform; hence, the value of ql decreases and reaches zero. Then, the half-width value $\Delta\Omega(T_e^D = 0)$ has no contribution from T_e^D . The difference $\Delta\Omega(T_e^D \neq 0) - \Delta\Omega(T_e^D = 0)$ includes a pure contribution from T_e^D .

Any contribution from the applied magnetic field is of course a concern. Note that an in-plane static magnetic field contributes no finite charge current generation or spin polarization [49], whereas the contribution from the applied magnetic field is negligible.

3. Spin pumping in a Weyl–Dirac semimetal

3.1. Model

We now consider spin pumping in a Weyl–Dirac semimetal subjected to magnetism. To do this, a Weyl–Dirac semimetal subjected to spin and momentum locking, such as a superlattice heterostructure constructed from a TI/normal insulator/TI [39, 46–48], is considered. The low-energy effective Hamiltonian describing the Weyl–Dirac semimetals that have a spin–exchange interaction is given by [50–52]

$$H = H_{\text{Weyl}} + H_{\text{ex}} + H_{\text{imp}}. \quad (20)$$

The first term takes the form

$$H_{\text{Weyl}} = \sum_k \Psi_k^\dagger [\hbar v_F \tau^z \otimes (\vec{k} - \tau^z \vec{b}) \cdot \sigma - \mu \tau^0 \otimes \sigma^0 - \mu^5 \tau^z \otimes \sigma^0] \Psi_k, \quad (21)$$

where $\Psi_k = (\Psi_{\uparrow,+}, \Psi_{\downarrow,+}, \Psi_{\uparrow,-}, \Psi_{\downarrow,-})$ is the annihilation operator of an electron with spin (\uparrow, \downarrow) and helicity $\tau(+, -)$ degrees of freedom; $\tau^{\alpha=0,x,y,z}$ and $\sigma^{\alpha=0,x,y,z}$ are Pauli matrices of the helicity and spin, respectively; v_F is the Fermi velocity; μ is the chemical potential of the Weyl–Dirac semimetal;

and \mathbf{b} and μ^5 denote the difference in position between each Weyl cone in momentum and energy space, respectively. In Dirac semimetals, we set $\mathbf{b} = 0$ and $\mu^5 = 0$.

The second term of Eq. (20) indicates the spin–exchange interaction:

$$H_{\text{ex}} = -J_{\text{ex}} \int dx \psi^\dagger [\tau^0 \otimes \vec{S} \cdot \vec{\sigma}] \psi, \quad (22)$$

where J_{ex} is the coefficient of the exchange interaction; and \mathbf{S} is the localized spin that depends on space and time in the Weyl semimetal. This exchange interaction is independent of the helicity index. H_{imp} shows the nonmagnetic impurity scattering in the Weyl–Dirac semimetal:

$$H_{\text{imp}} = \int dx u_{\text{imp}} \psi^\dagger [\tau^0 \otimes \sigma^0] \psi. \quad (23)$$

This Hamiltonian is similar to that on the surface of the TI—see Eq. (4). In the following calculations, H_{ex} and H_{imp} are treated as perturbations within the same formalism as laid out in Section 2.2. This treatment is allowed when the energy scale of the exchange interaction is smaller than the bandwidth of Eq. (21). Then, the low-energy effective Hamiltonian in Eq. (21) gives a good approximation.

3.2. Response function within the linear response to the exchange interaction

To calculate the charge and spin current within the linear response to H_{ex} , we use Green's functions. From Eq. (20) the charge current $\langle j^i \rangle$ ($i = x, y, z$) can be defined by

$$\langle j^i(x, t) \rangle = ev_F \langle \psi^\dagger(x, t) (\tau^z \otimes \sigma^i) \psi(x, t) \rangle. \quad (24)$$

where $\langle \rangle$ denotes the expectation value in Eq. (20). Such a charge current can be decomposed as $\langle \mathbf{j} \rangle = \langle \mathbf{j}_+ \rangle + \langle \mathbf{j}_- \rangle$, where $\langle \mathbf{j}_\pm \rangle = \pm ev_F \langle \Psi_\pm^\dagger \boldsymbol{\sigma} \Psi_\pm \rangle$ and $\Psi_\pm = (\Psi_{1,\pm}, \Psi_{2,\pm})$ is the annihilation operator around each helicity $\tau = \pm 1$. Since there is no mixing between $\Psi_{1,+}$ and $\Psi_{1,-}$ in the Hamiltonian in Eq. (20) the charge current around each helicity can be calculated separately. Because of spin–momentum locking in the Weyl–Dirac semimetal the charge current links to the spin polarization. The charge current of each helicity is proportional to the spin polarization of each helicity as

$$\langle j_\pm^i(x, t) \rangle = \pm \frac{ev_F}{2} \langle s_\pm^i(x, t) \rangle. \quad (25)$$

The spin current in the Weyl–Dirac semimetal can be defined from the Heisenberg equation for the spin operator:

$$\partial_t s_\alpha + \partial_i j_{s,\alpha}^i = T_{r,\alpha}, \tag{26}$$

where $j_{s,\alpha}^i$ is the spin current operator; and $T_{r,\alpha}$ is the spin relaxation term. Spin current density can also be decomposed into the spin current density of each helicity and can be calculated separately:

$$\langle j_{s,\alpha,\pm}^i \rangle = \pm \frac{\hbar v_F}{2} \delta_\alpha^i \langle \psi_\pm^\dagger \psi_\pm \rangle = \pm \frac{\hbar v_F}{2e} \delta_\alpha^i \langle \rho_\pm \rangle. \tag{27}$$

The superscript and subscripts of $j_{s,\alpha}^i$ denote the direction of flow and spin of the spin current of each helicity, respectively. The direction of spin is perfectly parallel to that of the flow, and the spin current density is proportional to the charge density of each helicity.

The relaxation term can also be decomposed by $\langle T_r \rangle = \langle T_{r,+} \rangle + \langle T_{r,-} \rangle$ and can be given by $\langle T_{r,\pm} \rangle$:

$$\langle T_{r,\pm} \rangle = \mp \frac{i\hbar v_F}{2} \varepsilon^{\alpha\beta} \langle \psi_\pm^\dagger \sigma^\beta (\partial^i \psi_\pm) - (\partial^i \psi_\pm^\dagger) \sigma^\beta \psi_\pm \rangle. \tag{28}$$

The charge and spin current can be obtained by calculating the response function (**Figure 4**):

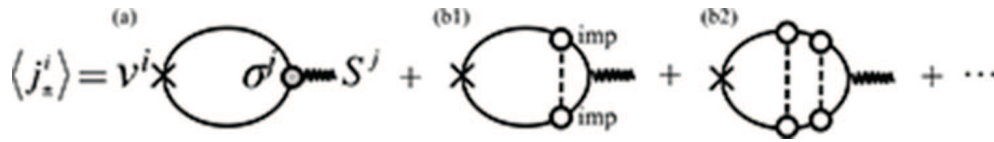


Figure 4. Diagrammatic representation of the charge current of each helicity within the linear response to the exchange interaction. The bold line is Green's function; v^i is the velocity operator; and S^j is the localized spin (wavy lines). (a) A bubble diagram without taking impurity scattering from the exchange interactions into account. (b1) and (b2) Bubble diagrams that take impurity scattering within the ladder approximation into account.

$$\begin{aligned} \langle j_\pm^i \rangle &= \pm \frac{ie\hbar v_F J_{\text{ex}}}{L^3} \sum_{\vec{q}, \Omega} e^{i(\Omega t - \vec{q} \cdot \vec{x})} \text{tr}[\sigma^i \Pi_\pm^j(\vec{q}, \Omega)] S_{\vec{q}, \Omega}^j, \\ \langle j_{s,\alpha,\pm}^i \rangle &= \mp \frac{i\hbar v_F J_{\text{ex}}}{2L^3} \delta_\alpha^i \sum_{\vec{q}, \Omega} e^{i(\Omega t - \vec{q} \cdot \vec{x})} \text{tr}[\Pi_\pm^j(\vec{q}, \Omega)] S_{\vec{q}, \Omega}^j, \end{aligned} \tag{29}$$

where \vec{q} and Ω are the momentum and frequency of the localized spin, respectively; L^3 is the volume of the system; and Π_\pm^j is the response function within the helicity index:

$$\Gamma_\pm^j \equiv n_c u_i^2 \sum_{\omega, \vec{k}} g_{\omega-\Omega/2, \vec{k}-\vec{q}/2, \pm}^R \sigma^j g_{\omega-\Omega/2, \vec{k}-\vec{q}/2, \pm}^A = \Gamma_\pm^{jn} \sigma^n. \tag{30}$$

where $f_{\omega} g_{\omega, k, \pm}^R = ([g_{\omega, k, \pm}^A]^\dagger) = [\hbar\omega/(2\pi) + \mu_{\pm} - \hbar v_F \mathbf{k} \cdot \boldsymbol{\sigma}/(2\pi) + i\hbar/(4\pi\tau_{\pm})]^{-1}$, and Λ_{\pm}^j are the Fermi distribution function, the retarded (advanced) Green's function, and the vertex correction of the ladder diagram at each helicity \pm , respectively; and τ_{\pm} is the relaxation time of nonmagnetic impurities in the material, which depends on the helicity, because it depends on the chemical potential μ_{\pm} . When $\Omega\tau_{e, \pm} \ll 1$ and $qv_F\tau_{e, \pm} \ll 1$ are satisfied the vertex function Λ_{\pm}^j is given by $\Lambda_{\pm}^j = [\Gamma_{\pm} + \Gamma_{\pm}^2 + \Gamma_{\pm}^3 + \dots]^{jn} \sigma^n = [(1 - \Gamma_{\pm})^{-1}]^{jn} \sigma^n$ with

$$\Gamma_{\pm}^j \equiv n_c u_i^2 \sum_{\omega, \mathbf{k}} g_{\omega - \Omega/2, \mathbf{k} - \mathbf{q}/2, \pm}^R \sigma^j g_{\omega + \Omega/2, \mathbf{k} + \mathbf{q}/2, \pm}^A = \Gamma_{\pm}^{jn} \sigma^n \quad (31)$$

where Γ_{\pm}^{jn} ($|\Gamma_{\pm}^{jn}| < 1$) is a 4×4 matrix ($j, n = 0, x, y, z$). As a result, Π_{\pm}^j can be represented by

$$\begin{pmatrix} \Pi_{\pm}^0 \\ \Pi_{\pm}^x \\ \Pi_{\pm}^y \\ \Pi_{\pm}^z \end{pmatrix} = \begin{pmatrix} \Pi_{\pm}^{00} & \Pi_{\pm}^{0x} & \Pi_{\pm}^{0y} & \Pi_{\pm}^{0z} \\ \Pi_{\pm}^{x0} & \Pi_{\pm}^{xx} & \Pi_{\pm}^{xy} & \Pi_{\pm}^{xz} \\ \Pi_{\pm}^{y0} & \Pi_{\pm}^{yx} & \Pi_{\pm}^{yy} & \Pi_{\pm}^{yz} \\ \Pi_{\pm}^{z0} & \Pi_{\pm}^{zx} & \Pi_{\pm}^{zy} & \Pi_{\pm}^{zz} \end{pmatrix} \begin{pmatrix} \sigma^0 \\ \sigma^x \\ \sigma^y \\ \sigma^z \end{pmatrix} \quad (32)$$

where the above matrix component ($m, m' = x, y, z$) is

$$\begin{aligned} \Pi_{\pm}^{00} &= -\frac{\Omega}{4\pi} \frac{2 + i\Omega\tau_{e, \pm}}{q^2 v_F^2 \tau_{e, \pm} / 2 + i\Omega}, \\ \Pi_{\pm}^{m0} = \Pi_{\pm}^{0m} &= \mp \frac{\Omega}{4\pi} \frac{iv_F q^m}{q^2 v_F^2 \tau_{e, \pm} / 2 + i\Omega}, \\ \Pi_{\pm}^{mm'} &= -\frac{\Omega}{4\pi} \left(1 - \frac{v_F^2 \tau_{e, \pm}^2 q^m q^{m'}}{q^2 v_F^2 \tau_{e, \pm} / 2 + i\Omega} \right). \end{aligned} \quad (33)$$

As a result, the charge current and spin current can be obtained by

$$\langle j_{\pm}^i \rangle = \pm \frac{ev_F J_{\text{ex}} \nu_{\pm}^{\text{WS}} \tau_{e, \pm}}{2} \partial_t \bar{S} - \frac{1}{6} v_F^2 \tau_{\pm} \bar{\nabla} \langle \rho_{\pm} \rangle, \quad (34)$$

$$\langle j_{s, \alpha, \pm}^i \rangle = \pm \frac{\hbar v_F}{2e} \delta_{\alpha}^i \langle \rho_{\pm} \rangle, \quad (35)$$

where ν_{\pm}^{WS} and $\langle \rho_{\pm} \rangle$ are the charge density of state and the induced charge density of each helicity, respectively:

$$\langle \rho_{\pm} \rangle = \mp \frac{1}{2} e v_F J_{\text{ex}} \nu_{\pm}^{\text{WS}} \tau_{e,\pm} \left(\vec{\nabla} \cdot \partial_t \langle \vec{S} \rangle_{\text{D},\pm} \right) \quad (36)$$

where $\langle \vec{S} \rangle_{\text{D},\pm}$ is the convolution between the localized spin and diffusive propagation of each helicity. $\langle \vec{S} \rangle_{\text{D},\pm}$ can be defined by

$$\begin{aligned} \langle \vec{S} \rangle_{\text{D},\pm} &\equiv \frac{1}{\tau_{e,\pm}} \int_{-\infty}^{\infty} dt' \int dx' D_{\text{W},\pm}(x-x', t-t') \vec{S}(x', t'), \\ D_{\text{W},\pm}(x-x', t-t') &= \frac{1}{L^3} \sum_{\vec{q}, \Omega} \frac{1}{q^2 v_F \tau_{e,\pm} / 2 + i\Omega} e^{i(\Omega t - \vec{q} \cdot \vec{x})}. \end{aligned} \quad (37)$$

Note that the above results are obtained when $\mathbf{b} = 0$. These results are easily generalized when $\mathbf{b} \neq 0$. Because \mathbf{b} behaves like a static Zeeman field acting on the whole of the band of H_{Weyl} it can shift as a result of Pauli paramagnetism. However, \mathbf{b} cannot drive a net current because \mathbf{b} is static [49]. On the other hand, the dynamics of the localized spin are only effective near the Fermi surface, the structure of which does not depend on \mathbf{b} . Therefore, we obtain the same charge and spin current in Eqs. (33)–(35) even when $\mathbf{b} \neq 0$.

3.3. Charge and spin current due to spin pumping effects

From the above results the total charge current can be given by

$$\langle j^i \rangle = \frac{e v_F J_{\text{ex}}}{2} (\nu_+^{\text{WS}} \tau_{e,+} - \nu_-^{\text{WS}} \tau_{e,-}) \partial_t S^i + \frac{e v_F^3 J_{\text{ex}}}{12} \nabla^i \left[\vec{\nabla} \cdot \partial_t (\nu_+^{\text{WS}} \tau_{e,+}^2 \langle \vec{S} \rangle_{\text{D},+} - \nu_-^{\text{WS}} \tau_{e,-}^2 \langle \vec{S} \rangle_{\text{D},-}) \right]. \quad (38)$$

The charge current is triggered by the dynamics of localized spin. The first term indicates the local term of the dynamics of localized spin. Its direction is parallel to $\partial_t \mathbf{S}$. The second term shows the nonlocal term, which is generated by the convolution between localized spin and the diffusion propagator. A nonzero nonlocal term is given when the spin texture of localized spin depends on space. Thus, the driving force needed to induce the charge current is the same as localized spin dynamics, which plays the role of driving the charge current on the surface of the TI. Note that the charge current in a Weyl–Dirac semimetal depends strongly on the valley index. When the difference between τ_+ and τ_- as well as between ν_+^{WS} and ν_-^{WS} is realized, there is a population imbalance between two of the bands of each helicity. Then, nonzero $\langle j \rangle$ is induced when $\nu_+^{\text{WS}} \tau_{e,+} \neq \nu_-^{\text{WS}} \tau_{e,-}$ or $\mu^5 \neq 0$.

Note that the property of the charge current at each helicity links to that of spin polarization because of spin–momentum locking. However, after summation of the indices of helicity the relation between total charge current and total spin polarization is changed. As a result, even in the absence of population imbalance, nonzero spin polarization can be given by Eq. (25) as

$$\langle s^i \rangle = \frac{J_{\text{ex}}}{2} (\nu_+^{\text{WS}} \tau_{e,+} + \nu_-^{\text{WS}} \tau_{e,-}) \partial_t S^i + \frac{v_F^2 J_{\text{ex}}}{24} \nabla^i \left[\vec{\nabla} \cdot \partial_t \left(\nu_+^{\text{WS}} \tau_{e,+}^2 \langle \vec{S} \rangle_{D,+} + \nu_-^{\text{WS}} \tau_{e,-}^2 \langle \vec{S} \rangle_{D,-} \right) \right]. \quad (39)$$

Local spin polarization is along $\partial_t S$ and nonlocal spin polarization is along the spatial gradient of $\partial_t(\partial^i S^i)$.

Total spin current can be represented from Eqs. (35) and (36) as

$$\langle j_{s,\alpha}^i \rangle = -\frac{\hbar v_F^2 J_{\text{ex}}}{4} \delta_\alpha^i \vec{\nabla} \cdot \partial_t \left[\nu_+^{\text{WS}} \tau_{e,+} \langle \vec{S} \rangle_{D,+} + \nu_-^{\text{WS}} \tau_{e,-} \langle \vec{S} \rangle_{D,-} \right]. \quad (40)$$

Total spin current can be generated by spatial divergence of localized spin dynamics, where localized spin is the convolution with diffusion. As a result, the spin current can be regarded as a nonlocal spin current. Note that a nonzero spin current is generated when localized spin depends on space. Such a spin current becomes nonzero even in the absence of population imbalance.

The nonlocal spin current in this case is obtained from the diffusive motion of spin density, which is driven by the dynamics of localized spin, where localized spin depends on space. The spin diffusive motion of each helicity can be given from Eqs. (25), (34), (37) as

$$\left(\partial_t - \frac{1}{2} v_F^2 \tau_{e,\pm} \right) \langle s_\pm^i \rangle = \frac{e v_F^3 \tau_{e,\pm}^2 J_{\text{ex}}}{2} \nu_\pm^{\text{WS}} \partial_t \nabla (\nabla \cdot S). \quad (41)$$

As a result, the diffusive motion of total spin becomes:

$$\left[\partial_t (\langle s_+^i \rangle + \langle s_-^i \rangle) - \frac{1}{2} v_F^2 (\tau_{e,+} \langle s_+^i \rangle + \tau_{e,-} \langle s_-^i \rangle) \right] = \frac{e v_F^3 J_{\text{ex}}}{2} (\tau_+^2 \nu_{e,+}^{\text{WS}} + \tau_-^2 \nu_{e,-}^{\text{WS}}) \partial_t \nabla (\nabla \cdot S) \quad (42)$$

Time-dependent and spatial-dependent localized spin, $\partial[\partial_t(\partial^i S^i)]$, triggers the diffusive motion of total spin density. When there is no population imbalance between each helicity, diffusive motion can accompany total spin density without any charge flow. Hence, a pure spin current can be generated.

4. Conclusion

Our results on the charge and spin current due to spin pumping on the surface of a three-dimensional TI (Section 2) [28] and in the bulk of a three-dimensional Weyl–Dirac semimetal (Section 3) [51] are summarized in this chapter.

Section 2 summarizes our results on spin pumping on the surface of a TI attached to an MI. The results are calculated using the standard Keldysh–Green function method within the linear response to the exchange interaction between the conduction spin and localized spin of an MI. The purpose of this work is to derive charge and spin current generation due to localized spin dynamics on the disordered surface of a TI; in particular, when the localized spin depends on space on the surface. The main results on the surface of a TI are summarized in **Table 1**. Time-dependent localized spin on the surface is a prerequisite to obtaining nonzero charge and spin current generation. Moreover, **Table 1** shows that when the spin texture is spatially inhomogeneous, not only the local charge but also the nonlocal charge and spin current are generated by time-dependent localized spin. The flow and spin polarization of the spin current are perfectly perpendicular to each other because of spin–momentum locking. The magnitude of the spin current is proportional to the charge density, which is induced by divergence between time-dependent localized spin and the diffusive propagator on the surface—see Eqs. (10) and (11). Such pumping effects are caused by time-dependent localized spin, which plays a role in driving the charge current and can be regarded as an effective electric field E_s^{TI} .

	$\langle j \rangle$	$\langle j_{s,\alpha}^i \rangle$	$\langle s \rangle$	$\langle p \rangle$	Ref.
Local	$z \times \partial_t S^{\text{II}}$		$\partial_t S^{\text{II}}$		[29-31]
Nonlocal	$\nabla[\nabla \times \partial_t S^{\text{II}}]_z$	$\epsilon^{z\alpha i}[\nabla \times \partial_t S^{\text{II}}]_z$	$\nabla[\nabla \times \partial_t S^{\text{II}}]_z$	$[\nabla \times \partial_t S^{\text{II}}]_z$	This work [28]
Driving force	$z \times \epsilon_s^{\text{TI}}$	$[\nabla \times \epsilon_s^{\text{TI}} D]_z$	$z \times \epsilon_s^{\text{TI}}$	$[\nabla \times \epsilon_s^{\text{TI}} D]_z$	This work [28]
$\epsilon_s^{\text{TI}} \equiv -\frac{J_{\text{ex}}}{ev_F} \partial_t S^{\text{II}}$	$\nabla[\nabla \times \langle \epsilon_s^{\text{TI}} \rangle_D]_z$		$\nabla[\nabla \times \langle \epsilon_s^{\text{TI}} \rangle_D]_z$		

Table 1. Brief summary of the charge current, spin current, spin, and charge density induced by localized spin dynamics on the disordered surface of a TI. The charge current and spin density have both a local and nonlocal contribution. The spin current and charge density are described by the nonlocal contribution.

Recently, it has been reported that the localized spin texture at the junction of the TI/MI is spatially inhomogeneous [34]. We suppose that the spin current we have obtained at the junction is generated when the spin texture moves temporally.

On the basis of these results, in Section 2.3 we discussed a way of detecting the charge current and spin current induced on the surface of a TI attached to an MI by using ferromagnetic resonance. We assume that the dynamics of localized spin is triggered by the applied static and AC magnetic field of the microwave. The dynamics of the localized spin induced both the charge current and the spin current. Such induced currents are related to spin density, and spin polarization acts on the localized spin in much the same way as spin torque—see Eq. (14). Hence, the half-width of ferromagnetic resonance changes as shown in **Figure 3**.

Spin pumping in a Weyl–Dirac semimetal hosting massless Weyl–Dirac fermions is summarized in section 3. The results are obtained within the same formalism as laid out in Sections 2.1 and 2.2. The charge and spin current as well as the charge and spin density are given in **Table 2**. Semimetals are subject to spin–momentum locking. The spin direction of Weyl–Dirac fermions brought about by spin–momentum locking is perfectly parallel/antiparallel to its momentum and its locking is determined by the helicity degrees of freedom of Weyl–Dirac fermions. As a result, the charge current and spin polarization induced depend on the helicity indices. Eqs. (38) and (39) show that localized spin dynamics induces the charge current and spin polarization, respectively; hence, localized spin plays the role of an effective electric field $E_{s,\pm}^{\text{WDS}}$ acting on electrons [51]. Moreover, $E_{s,\pm}^{\text{WDS}}$ depends on the helicity index, whereas total charge current is proportional to μ^5 . As a result, a nonzero charge current is generated when there is population imbalance between each helicity. On the other hand, localized spin dynamics also drives the spin current when localized spin depends on time and position in a Weyl–Dirac semimetal. The spin current is finite even in the absence of population imbalance. Then, the spin current does not accompany charge flow. These results may be of use to next-generation spintronics devices based on Weyl–Dirac semimetals.

	$\langle j_{\pm} \rangle \propto \langle S_{\pm} \rangle$	$\langle j_{s,\alpha,\pm}^i \rangle \propto \delta_{i,\alpha} \langle \rho_{\pm} \rangle$	Ref.
Local	$\mp \partial_t S$		[51]
Nonlocal	$\mp \nabla [\nabla \cdot \partial_t S_{D,\pm}]$	$\delta_{i,\alpha} \nabla \cdot \partial_t \langle s \rangle_{D,\pm}$	[51]
Driving force $\varepsilon_{s,\pm}^{\text{WDS}} \equiv \mp \frac{J_{ex}}{ev_p} \partial_t S$	$\varepsilon_{s,\pm}^{\text{WDS}}$ and $\nabla [\nabla \cdot (\varepsilon_s^{\text{WDS}})_{D,\pm}]$	$\nabla \cdot (\varepsilon_s^{\text{WDS}})_{D,\pm}$	This work [51]
Total	$\langle j \rangle_{\text{local}} \propto \mu^5 \partial_t S$ $\langle j \rangle_{\text{nonlocal}} \propto \partial_t \nabla [\nabla \cdot (\langle s \rangle_{D,+} - \langle s \rangle_{D,-})]$	$\langle j_{s,\alpha}^i \rangle_{\text{nonlocal}} \propto \delta_{i,\alpha} \partial_t \nabla \cdot (\langle s \rangle_{D,+} + \langle s \rangle_{D,-})$	This work

Table 2. Brief summary on charge and spin current generation by spin pumping in a Weyl–Dirac semimetal with the dynamics of localized spin, where \pm denotes the helicity index. Because of spin–momentum locking the charge (spin) current is proportional to the spin (charge) density with each helicity. Time-dependent localized spin drives the local and nonlocal charge and spin current. The nonzero population imbalance between each helicity μ^5 is a prerequisite to obtaining the nonzero charge current. The nonzero spin current (charge density) is triggered by time-dependent and spatial-dependent localized spin dynamics even when $\mu^5 = 0$.

Acknowledgements

This work was supported by a Grant-in-Aid for JSPS Fellows (Grant No. 13J03141), by a Grant-in-Aid for Challenging Exploratory Research (Grant No. 15K13498), and by the Core Research for Evolutional Science and Technology (CREST) of Japan Science.

Author details

Katsuhisa Taguchi

Address all correspondence to: taguchi@rover.nuap.nagoya-u.ac.jp

Department of Applied Physics, Nagoya University, Nagoya, Japan

References

- [1] Tserkovnyak Y, Brataas A, Bauer GEW. Enhanced gilbert damping in thin ferromagnetic films. *Phys Rev Lett.* 2002;88(11):117601. DOI: 10.1103/PhysRevLett.88.117601
- [2] Saitoh E, Ueda M, Miyajima H, Tatara G. Conversion of spin current into charge current at room temperature: Inverse spin-Hall effect. *Appl Phys Lett.* 2006;88(18):13–6. DOI: 10.1063/1.2199473
- [3] Hasan MZ, Kane CL. Colloquium: Topological insulators. *Rev Mod Phys.* 2010;82(4):3045–67. DOI:10.1103/RevModPhys.82.3045
- [4] Qi XL, Zhang SC. Topological insulators and superconductors. *Rev Mod Phys.* 2011;83(4). DOI: 10.1103/RevModPhys.83.1057
- [5] Ando Y. Topological insulator materials. *J Phys Soc Japan.* 2013;82(10):1–32. DOI: 10.7566/JPSJ.82.102001
- [6] Hsieh D, Xia Y, Qian D, Wray L, Dil JH, Meier F, et al. A tunable topological insulator in the spin helical Dirac transport regime. *Nature.* 2009;460(7259):1101–5. DOI: 10.1038/nature08234
- [7] Yokoyama T, Tanaka Y, Nagaosa N. Anomalous magnetoresistance of a two-dimensional ferromagnet/ferromagnet junction on the surface of a topological insulator. *Phys Rev B.* 2010;81(12):3–6. DOI: 10.1103/PhysRevB.81.121401
- [8] Schwab P, Raimondi R, Gorini C. Spin-charge locking and tunneling into a helical metal. *Europhysics Lett.* 2011;93(6):67004. DOI: 10.1209/0295-5075/93/67004
- [9] Mondal S, Sen D, Sengupta K, Shankar R. Magnetotransport of Dirac fermions on the surface of a topological insulator. *Phys Rev B.* 2010;82(4):1–11. DOI: 10.1103/PhysRevB.82.045120
- [10] Ma MJ, Jalil MBA, Tan SG, Li Y, Siu ZB. Spin current generator based on topological insulator coupled to ferromagnetic insulators. *AIP Adv.* 2012;2(3). DOI: 10.1063/1.4751255

- [11] Kong BD, Semenov YG, Krowne CM, Kim KW. Unusual magnetoresistance in a topological insulator with a single ferromagnetic barrier. *Appl Phys Lett*. 2011;98(24):96–9. DOI: 10.1103/PhysRevB.89.201405
- [12] Kandala A, Richardella A, Rench DW, Zhang DM, Flanagan TC, Samarth N. Growth and characterization of hybrid insulating ferromagnet–topological insulator heterostructure devices. *Appl Phys Lett*. 2013;103(20):2011–5. DOI: 10.1063/1.4831987
- [13] Taguchi K, Yokoyama T, Tanaka Y. Giant magnetoresistance in the junction of two ferromagnets on the surface of diffusive topological insulators. *Phys Rev B*. 2014;89(8):1–5. DOI: 10.1103/PhysRevB.89.085407
- [14] Fischer MH, Vaezi A, Manchon A, Kim E-A. Spin–Torque generation in topological–insulator-based Heterostructures. *Phys Rev B*. 2016;93(12):1-4. DOI: 10.1103/PhysRevB.93.12530
- [15] Jamali M, Lee JS, Lv Y, Zhao Z, Samarth N, Wang JP. Room Temperature Spin Pumping in Topological Insulator Bi₂Se₃. [Internet.] 2014. Available from: <http://arxiv.org/abs/1407.7940>
- [16] Qi XL, Hughes TL, Zhang SC. Topological field theory of time-reversal invariant insulators. *Phys Rev B*. 2008;78(19):1–43. DOI: 10.1103/PhysRevB.78.195424
- [17] Garate I, Franz M. Inverse spin-galvanic effect in the interface between a topological insulator and a ferromagnet. *Phys Rev Lett*. 2010;104(14):1–4. DOI: 10.1103/PhysRevLett.104.146802
- [18] Nomura K, Nagaosa N. Electric charging of magnetic textures on the surface of a topological insulator. *Phys Rev B*. 2010;82(16):3–6. DOI: 10.1103/PhysRevB.82.161401
- [19] Ueda HT, Takeuchi A, Tataro G, Yokoyama T. Topological charge pumping effect by the magnetization dynamics on the surface of three-dimensional topological insulators. *Phys Rev B*. 2012;85(11):1–6. DOI: 10.1103/PhysRevB.85.115110
- [20] Linder J. Improved domain-wall dynamics and magnonic torques using topological insulators. *Phys Rev B*. 2014;90(4):1–5. DOI: 10.1103/PhysRevB.90.041412
- [21] Taguchi K, Shintani K, Tanaka Y. Electromagnetic effect on disordered surface of topological insulators. *J Magn Magn Mater*. 2015;400:188–10. DOI: 10.1103/PhysRevB.92.035425
- [22] Burkov AA, Hawthorn DG. Spin and charge transport on the surface of a topological insulator. *Phys Rev Lett*. 2010;105(6):6–9. DOI: 10.1103/PhysRevLett.105.066802
- [23] Fujimoto J, Sakai A, Kohno H. Ultraviolet divergence and Ward–Takahashi identity in a two-dimensional Dirac electron system with short-range impurities. *Phys Rev B*. 2013;87(8):1–5. DOI: 10.1103/PhysRevB.87.085437
- [24] Sakai A, Kohno H. Spin torques and charge transport on the surface of topological insulator. *Phys Rev B*. 2014;89(16). DOI: 10.1103/PhysRevB.89.165307

- [25] Liu X, Sinova J. Reading charge transport from the spin dynamics on the surface of a topological insulator. *Phys Rev Lett*. 2013;111(16):1–5. DOI: 10.1103/PhysRevLett.111.166801
- [26] Tserkovnyak Y, Loss D. Thin-film magnetization dynamics on the surface of a topological insulator. *Phys Rev Lett*. 2012;108(18):1–5. DOI: 10.1103/PhysRevLett.108.187201
- [27] Tserkovnyak Y, Pesin DA, Loss D. Spin and orbital magnetic response on the surface of a topological insulator. *Phys Rev B*. 2015;91(4):041121. DOI: 10.1103/PhysRevB.91.041121
- [28] Taguchi K, Shintani K, Tanaka Y. Spin-charge transport driven by magnetization dynamics on disordered surface of doped topological insulators. *Phys Rev B*. 2015;035425:1–34. DOI: 10.1103/PhysRevB.92.035425 [Figure 4(b) in reference [28] is a misprint: The values 0.38, 0.34, and 0.30 on the vertical axis in the figure should be 0.038, 0.034, and 0.030, respectively. Figure 3(c) in this chapter is revised.]
- [29] Semenov YG, Duan X, Kim KW. Voltage-driven magnetic bifurcations in nanomagnet–topological insulator heterostructures. *Phys Rev B*. 2014;89(20):1–5. DOI: 10.1103/PhysRevB.89.201405
- [30] Deorani P, Son J, Banerjee K, Koirala N, Brahlek M, Oh S, et al. Observation of inverse spin Hall effect in bismuth selenide. *Phys Rev B*. 2014;094403:1–19. DOI: 10.1103/PhysRevB.90.094403
- [31] Shiomi Y, Nomura K, Kajiwara Y, Eto K, Novak M, Segawa K, et al. Spin–electricity conversion induced by spin injection into topological insulators. *Phys Rev Lett*. 2014;113(19):7–11. DOI: 10.1103/PhysRevLett.113.196601
- [32] Mizukami S, Ando Y, Miyazaki T. Effect of spin diffusion on Gilbert damping for a very thin permalloy layer in Cu/permalloy/Cu/Pt films. *Phys Rev B*. 2002;66(10):1–9. DOI: 10.1103/PhysRevB.66.104413
- [33] Gilbert TL. Classics in magnetic: A phenomenological theory of damping in ferromagnetic materials. *IEEE Trans Magn*. 2004;40(6):3443–9. DOI: 10.1109/TMAG.2004.836740
- [34] Wei P, Katmis F, Assaf BA, Steinberg H, Jarillo-Herrero P, Heiman D, et al. Exchange-coupling-induced symmetry breaking in topological insulators. *Phys Rev Lett*. 2013;110(18):1–5. DOI: 10.1103/PhysRevLett.110.186807
- [35] Coop G, Przeworski M, Wall JD, Frisse LA, Hudson RR, Di Rienzo A, et al. Observation of skyrmions in a multiferroic material. *Science*. 2012;336(April):198–201. DOI: 10.1126/science.1214143
- [36] White JS, Prša K, Huang P, Omrani AA, Živković I, Bartkowiak M, et al. Electric-field-induced skyrmion distortion and giant lattice rotation in the magnetoelectric insulator Cu₂OSeO₃. *Phys Rev Lett*. 2014;113(10):1–5. DOI: 10.1103/PhysRevLett.113.107203

- [37] Murakami S. Phase transition between the quantum spin Hall and insulator phases in 3D: Emergence of a topological gapless phase. *New J Phys.* 2007;9. DOI: 10.1088/1367-2630/9/9/356
- [38] Yang B, Nagaosa N. Classification of stable three-dimensional Dirac semimetals with nontrivial topology. *Nat Commun.* 2014;5:4898. DOI: 10.1038/ncomms5898
- [39] Burkov AA, Balents L. Weyl semimetal in a topological insulator multilayer. *Phys Rev Lett.* 2011;107(12):1–4. DOI: 10.1103/PhysRevLett.107.127205
- [40] Brahlek M, Bansal N, Koirala N, Xu SY, Neupane M, Liu C, et al. Topological-metal to band-insulator transition in $(\text{Bi}_{1-x}\text{In}_x)_2\text{Se}_3$ thin films. *Phys Rev Lett.* 2012;109(18):1–5. DOI: 10.1103/PhysRevLett.109.186403
- [41] Wu L, Brahlek M, Valdés Aguilar R, Stier AV, Morris CM, Lubashevsky Y, et al. A sudden collapse in the transport lifetime across the topological phase transition in $(\text{Bi}_{1-x}\text{In}_x)_2\text{Se}_3$. *Nat Phys.* 2013;9(7):410–4. DOI: 10.1038/nphys2647
- [42] Liu ZK, Jiang J, Zhou B, Wang ZJ, Zhang Y, Weng HM, et al. A stable three-dimensional topological Dirac semimetal Cd_3As_2 . *Nat Mater.* 2014;13(7):677–81. DOI: 10.1038/nmat3990
- [43] Neupane M, Xu S-Y, Sankar R, Alidoust N, Bian G, Liu C, et al. Observation of a three-dimensional topological Dirac semimetal phase in high-mobility Cd_3As_2 . *Nat Commun.* 2014;05:3786- May 7;5. DOI: 10.1038/ncomms4786
- [44] Novak M, Sasaki S, Segawa K, Ando Y. Large linear magnetoresistance in the Dirac semimetal TlBiSSe . *Phys Rev B.* 2015;91(4):1–5. DOI: 10.1103/PhysRevB.91.041203
- [45] Huang S-M, Xu S-Y, Belopolski I, Lee C-C, Chang G, Wang B, et al. A Weyl Fermion semimetal with surface Fermi arcs in the transition metal mononictide TaAs class. *Nat Commun.* 2015;6:7373. DOI: 10.1038/ncomms8373
- [46] Tominaga J, Kolobov AV, Fons P, Nakano T, Murakami S. Ferroelectric order control of the Dirac–semimetal phase in $\text{GeTe-Sb}_2\text{Te}_3$ superlattices. *Adv Mater Interfaces.* 2013;1:1-7. DOI: 10.1002/admi.201300027
- [47] Zyuzin AA, Wu S, Burkov AA. Weyl semimetal with broken time reversal and inversion symmetries. *Phys Rev B.* 2012;85(16):1–9. DOI: 10.1103/PhysRevB.85.165110
- [48] Zyuzin AA, Burkov AA. Topological response in Weyl semimetals and the chiral anomaly. *Phys Rev B.* 2012;86(11):1–8. DOI: 10.1103/PhysRevB.86.115133
- [49] Vazifeh MM, Franz M. Electromagnetic response of Weyl semimetals. *Phys Rev Lett.* 2013;111(2):1–5. DOI: 10.1103/PhysRevLett.111.027201
- [50] Taguchi K. Equilibrium axial current due to a static localized spin in Weyl semimetals. *J Phys Conf Ser.* 2014;568(5):052032. DOI: 10.1088/1742-6596/568/5/052032

- [51] Taguchi K, Tanaka Y. Axial current driven by magnetization dynamics in Dirac semimetals. *Phys Rev B*. 2015;91(5):1–5. DOI:10.1103/PhysRevB.91.054422
- [52] Nomura K, Kurebayashi D. Charge-induced spin torque in anomalous Hall ferromagnets. *Phys Rev Lett*. 2015;115(12):1–5. DOI: 10.1103/PhysRevLett.115.127201
- [53] Chan C-K, Lee P A, Burch KS, Han JH, Ran Y. When chiral photons meet chiral fermions: Photoinduced anomalous Hall effects in Weyl semimetals. *Phys Rev Lett*. 2015;115(7):1–5. DOI: 10.1103/PhysRevLett.115.026805
- [54] Taguchi K, Imaeda T, Sato M, Tanaka Y. Photovoltaic chiral magnetic effect in a Weyl semimetal. *Phys Rev B(R)*. 2016;93(20):1–5. DOI: 10.1103/PhysRevB.93.201202
- [55] Haug H, Jauho A-P. *Quantum Kinetics in Transport and Optics of Semiconductors*. [Internet.] 2008. 362 pp. Available from: <http://www.springer.com/physics/complexity/book/978-3-540-73561-8>
- [56] Tokura Y, Kida, N. Dynamical magnetoelectric effects in multiferroic oxides. *Phil. Trans. R. Soc. A*. 2011;369:3679–3694. DOI: 10.1098/rsta.2011.0150